General formula for bi-aspheric singlet lens design free of spherical aberration

Article *in* Applied Optics · October 2018

DOI: 10.1364/AO.57.009341

2 authors:

Rafael G. González-Acuña
Huawei Technologies
136 PUBLICATIONS **466** CITATIONS
SEE PROFILE

Hector Alejandro Chaparro Romo
Independient
56 PUBLICATIONS **237** CITATIONS
SEE PROFILE

Research Article Vol. 57, No. 31 / 1 November 2018 / Applied Optics 9341

applied optics

General formula for bi-aspheric singlet lens design free of spherical aberration

Rafael G. González-Acuña[1,*] and Héctor A. Chaparro-Romo[2,3]

[1]Optics Center, Physics Department, Tecnológico de Monterrey Garza Sada 2501, Monterrey, N.L. 64849, Mexico
[2]Av. Universidad No. 3000, Universidad Nacional Autónoma de México, C.U., Mexico City, Mexico
[3]e-mail: moxaika@live.com
*Corresponding author: rafael123.90@hotmail.com

Received 24 August 2018; revised 3 October 2018; accepted 3 October 2018; posted 5 October 2018 (Doc. ID 343158); published 25 October 2018

In this paper, we present a rigorous analytical solution for the bi-aspheric singlet lens design problem. The input of the general formula presented here is the first surface of the singlet lens; this surface must be continuous and such that the rays inside the lens do not cross each other. The output is the correcting second surface of the singlet; the second surface is such that the singlet is free of spherical aberration.

https://doi.org/10.1364/AO.57.009341

1. INTRODUCTION

The design of optical systems with aspheric surface has the goal to strongly reduce spherical aberration. Spherical aberration on lenses has been extensively studied by Ref. [1]. Luneberg [2] established a method for computing the shape of the second surface from an initial first surface that introduces spherical aberration, which he described just for special cases. Many authors proposed a lens design with two aspheric surfaces to correct spherical aberration [3,4].

The problem of the design of a singlet free of spherical aberration with two aspheric surfaces is also known as the Wasserman and Wolf problem [5]. The problem has been solved with a numerical approach by Ref. [6]. Recently, Ref. [7] has shown a rigorous analytical solution of a singlet lens free of spherical aberration for the special case when the first surface is flat or conical. Since its publication, several works inspired by its solution have emerged [7–12], all of them free of spherical aberration. The solution has six different signs; therefore, it is a set of $2^6 = 64$ possible solutions, where only one is right. We test the formula provided by those in Ref. [7], when the first surface is not flat or conic, and the equation system does not give correct answers.

In this paper, we present a rigorous analytical solution for the design of lenses free of spherical aberration. The solution presented here has just one sign; therefore, it is a set of just two possible solutions. Our solution is robust because the set of solutions is valid for negative and positive refraction indices. The model allows use of continuous functions, such that the rays inside the lens do not cross each other. This model will compute the second surface in order to correct the spherical aberration produced by the first surface.

2. MATHEMATICAL MODEL

The goal is to determine the shape of the second surface (r_b, z_b), given a first surface (r_a, z_a), in order to correct the spherical aberration generated by the first surface. Therefore the objective is to find (r_b, z_b) given (r_a, z_a), where r_a is the only independent variable, and z_b, r_b, and z_a are functions of r_a. The origin of the coordinate system is located at the center of the input surface $z_a(0) = 0$.

We assume that the singlet lens has refraction index n and is radially symmetric. At the center, the singlet lens has thickness t. The distance from the object to the first surface is t_a. The distance from the second surface to the image is t_b, as can be seen in Fig. 1.

The first fundamental equation for this model is the vector form of the Snell's law:

$$\boldsymbol{v}_2 = \frac{1}{n}[\boldsymbol{n}_a \times (-\boldsymbol{n}_a \times \boldsymbol{v}_1)] - \boldsymbol{n}_a \sqrt{1 - \frac{1}{n^2}(\boldsymbol{n}_a \times \boldsymbol{v}_1) \cdot (\boldsymbol{n}_a \times \boldsymbol{v}_1)}, \tag{1}$$

where $\boldsymbol{v}_1$ is the unitary vector of the incident ray, $\boldsymbol{v}_2$ is the unitary vector of the refracted ray, and $\boldsymbol{n}_a$ is the normal vector of the first surface, as seen in Fig. 2.

The unitary vectors written of the first surface are

$$\begin{cases} \boldsymbol{v}_1 = \frac{[r_a, (z_a - t_a), 0]}{\sqrt{r_a^2 + (z_a - t_a)^2}}, \\ \boldsymbol{v}_2 = \frac{[r_b - r_a, z_b - z_a, 0]}{\sqrt{(r_b - r_a)^2 + (z_b - z_a)^2}}, \\ \boldsymbol{n}_a = \frac{[z_a', -1, 0]}{\sqrt{1 + z_a'^2}}, \end{cases} \tag{2}$$

where z_a' is the derivative with respect to r_a of the sagitta of the first surface.

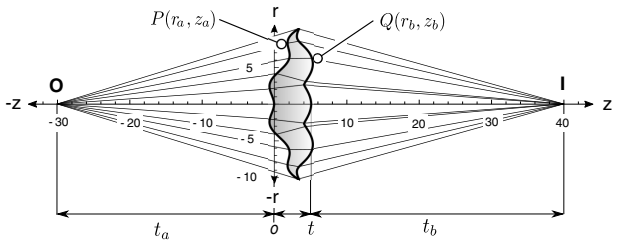

Fig. 1. Diagram of a singlet lens free of spherical aberration. The first surface is given by (r_a, z_a), and the second surface is given by (r_b, z_b). The distance between the first surface and the object is t_a, the thickness at the center of the lens is t, and the distance between the second surface and the image is t_b.

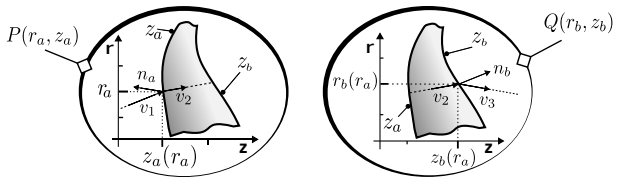

Fig. 2. *Left:* Zoom at point P of Fig. (1); three unitary vectors can be seen: $\boldsymbol{v}_1$ is the unitary vector of the incident ray, $\boldsymbol{v}_2$ is the unitary vector of the refracted ray, and $\boldsymbol{n}_a$ is the normal vector of the first surface. *Right:* Zoom at point Q of Fig. (1); unitary vectors of the second surface can be seen: $\boldsymbol{v}_2$ is the unitary vector of the incited ray, $\boldsymbol{v}_3$ is the unitary vector of the refracted ray, and $\boldsymbol{n}_b$ is the normal vector of the second surface.

Replacing Eq. (2) in Eq. (1) and separating the Cartesian components, we get the following expressions for the direction cosines r_i, z_i of the vector:

$$\begin{cases} r_i \equiv \frac{r_b - r_a}{\Psi} = \frac{(z_a - t_a)z_a' + r_a}{n\sqrt{r_a^2 + (t_a - z_a)^2(1 + z_a'^2)}} - z_a'\Phi, \\ z_i \equiv \frac{z_b - z_a}{\Psi} = \frac{(r_a + (z_a - t_a)z_a')z_a'}{n\sqrt{r_a^2 + (t_a - z_a)^2(1 + z_a'^2)}} + \Phi, \\ \text{with,} \\ \Psi = \sqrt{(z_b - z_a)^2 + (r_b - r_a)^2} \\ \Phi = \frac{\sqrt{1 - \frac{(r_a + (z_a - t_a)z_a')^2}{n^2(r_a^2 + (t_a - z_a)^2)(1 + z_a'^2)}}}{\sqrt{1 + z_a'^2}} \end{cases} \tag{3}$$

and, evidently, $z_i^2 + r_i^2 = 1$. Relations (3) come from the application of the Snell law for an arbitrary ray striking the singlet lens at point (r_a, z_a). Note that the expressions in the right sides of Eq. (3) are fully expressed in terms of the coordinates of the input surface, i.e., $z_i = z_i(r_a, z_a)$ and so on.

Now let us focus on the Fermat's principle, which is the second fundamental equation of our model. We assume for a spherical aberration-free singlet lens, the optical path of any non-central ray must be equal to the optical path of the axial ray:

$$\begin{aligned} -t_a + nt + t_b = &-\text{sgn}(t_a)\sqrt{r_a^2 + (z_a - t_a)^2} \\ &+ n\sqrt{(r_b - r_a)^2 + (z_b - z_a)^2} \\ &+ \text{sgn}(t_b)\sqrt{r_b^2 + (z_b - t - t_b)^2}, \end{aligned} \tag{4}$$

where $\text{sgn}(t_a)$ and $\text{sgn}(t_b)$ are the sign functions of the variable t_a or t_b, respectively.

Now we have a system of three equations: two components of vector form of Snell's law, Eq. (3), and Fermat's principle, Eq. (4). Furthermore, we have two unknowns, r_b and z_b. The solution of the system is

$$\begin{cases} r_b = \frac{r_i(z_b - z_a)}{z_i} + r_a, \\ z_b = \frac{h_0 + s_1\sqrt{z_i^2[-2nf_i(z_i(z_a - t_b + t(z_i - 1)) + r_a r_i + tr_i^2)} \\ \qquad -(r_i(-z_a + t_b + t) + r_a z_i)^2 + f_i^2 + h_1 n^2]}{1 - n^2} \end{cases} \tag{5}$$

where s_1 is the only sign; it comes from the fact that when the refraction index is positive, the rays are refracted to the opposite direction when the refraction index is negative. Also, we define the following auxiliary variables:

$$\begin{cases} f_i = -\text{sgn}(t_a)\sqrt{r_a^2 + (t_a - z_a)^2} + t_a - t_b, \\ h_0 = nf_i z_i - n^2(tz_i + z_a) + r_i^2 z_a - r_a r_i z_i + z_i^2(t + t_b), \\ h_1 = r_a^2 + 2r_a r_i t + (t_b - z_a)^2 + t^2(r_i^2 + (-1 + z_i)^2) \\ \qquad - 2t(t_b - z_a)(-1 + z_i). \end{cases} \tag{6}$$

Equation (5) is the most important result in this work. It could look cumbersome, but it is notorious that it could be expressed in closed form for an almost arbitrary freeform input surface. The condition for the validity of Eq. (5) is that the surface normal should be perpendicular to the tangent plane to the input surface at the origin, and the rays do not cross each other inside the lens.

From a topological point of view, since the singlet lens is a homogeneous optical element, the input and output surfaces are simply connected sets on $\mathbb{R}^2$ that can be defined as

$$\begin{aligned} \Omega_a &= \{(r_a, z_a) \in \mathbb{R}^2 | z_a < z_b\}, \\ \Omega_b &= \{(r_b, z_b) \in \mathbb{R}^2 | z_b > z_a\}, \end{aligned} \tag{7}$$

where Ω_a is homeomorphic to Ω_b, and both surfaces are topologically equivalent. Thus, there exists a continuous and bijective function f, such that $f{:}\Omega_a \to \Omega_b$, and whose inverse f^{-1} is continuous.

There are many functions f that map both sets, but there is only one that is physically valid and corresponds to the one that satisfies the variational Fermat principle of minimum optical length, which is constant. In our case, f is given by Eq. (5). The uniqueness of f has as consequence that the Snell law is automatically fulfilled at the second interface z_b as well.

Now, since f is continuous, it means that f maps open balls from Ω_a to Ω_b, then the ray neighborhoods are preserved. Therefore, the validity of Eq. (5) also requires that the rays do not intersect each other inside the lens because, in the case when the rays inside cross each other, Ω_b overlaps itself, and then Ω_b is no longer a simple connected set; it is not homeomorphic with respect to Ω_a, the vicinity of the neighborhoods is not preserved, and finally we do not have a homogeneous optical element.

3. RESULTS AND EXAMPLES

In this section, we report some illustrative results of Eq. (5), in six different contexts, with the objective to show the capacity of our model. We compare our results with Ref. [7], then we inject the model with functions that have never been evaluated, and we observe that they satisfy the optical path conditions; we load the system with a fixed input function and change the distance between the image and the second surface, in order to show that the model adjusts the second surface and corrects the spherical aberration. Then, we show an example of negative refraction index, and an example when the object is at minus infinity, $t_a = -\infty$, and finally we compute the efficiency of Eq. (5).

A. Comparison Between Solutions

Table 1 shows the results of the comparison of the solution given in Ref. [7] with ours, for plane, spherical, parabolic, and cosine cases. The sagitta for each surface corresponds to flat $z_a = 0$, parabolic-aspheric case $z_a = r_a^2/200$, spheric-aspheric case $z_a = 100 - \sqrt{100^2 - r_a^2}$, and cosine-aspheric case $z_a = \cos(r_a/3)$. In addition, the error difference between both solutions is reported.

The difference is computed by the following formula:

$$\text{RS Error} = \sum_N \frac{(z_b - z_{bc})^2}{N}, \tag{8}$$

where N is the number of samples, z_b is the sagitta of Eq. (5), and z_{bc} is the sagitta of the solution of Ref. [7]. We evaluate the values of the first quadrant because the solutions provided by Ref. [7] are not symmetric and fail in the second quadrant. For the evaluation, we use a sample of $N = 500$.

With the data in Table 1, we can argue that our solution in the first quadrant and for conic surfaces is equal to the solution of Ref. [7]. Also, it is important to mention that all this computation was made without the point $z_{bc}(0)$, because in the method of Ref. [7], that point diverges and for our method at the same point, we have $z_b(0) = t + z_a(0)$.

Table 1. Benchmark of Resolver Power Between Analytical Solutions to Design of Singlet Lenses Free of Spherical Aberration

	Solution According to J.C.V.E	Solution According to R.G.G.A. and H.A.C.R.
(1)	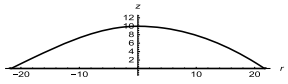	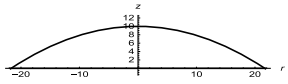
(2)	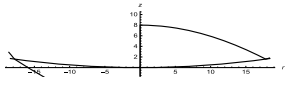	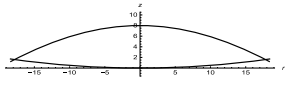
(3)	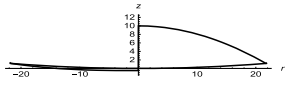	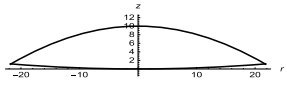
(4)	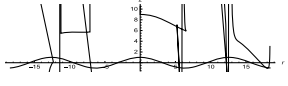	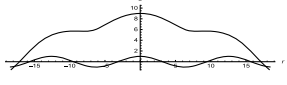

Basic configuration for all cases: $n = 1.5$ and $s_1 = 1$ for (1) flat, (2) spherical, (3) paraboloid, and (4) cosine; we have: (1) $t_a = -70$ mm, $t = 10$ mm, $t_b = 75$ mm, RS $= 1.20 \times 10^{-29}$. (2) $t_a = -70$ mm, $t = 8$ mm, $t_b = 80$ mm, RS $= 4.54 \times 10^{-28}$. (3) $t_a = -80$ mm, $t = 10$ mm, $t_b = 100$ mm, RS $= 1.75 \times 10^{-28}$. (4) $t_a = -70$ mm, $t = 8$ mm, $t_b = 80$ mm, RS = [redacted].

B. Gallery of Lenses with New Solution

This time, the first surfaces are not conic. The model is robust enough that it can admit nonstandard functions as first surfaces; the sagittae of the first functions of Fig. 3 are

$$\begin{cases} a)\ z_a = \begin{cases} \exp(r_a) + J_0(r_a) & \text{with, } r_a < 0 \\ \exp(-r_a) + J_0(r_a) & \text{with, } r_a \geq 0, \end{cases} \\ b)\ z_a = \frac{1}{18} r_a^2 + \cos\left(\frac{r_a}{2}\right), \\ c)\ z_a = 5\cos\left(\frac{r_a}{5}\right), \\ d)\ z_a = -\frac{1}{18} r_a^2 + \cos\left(\frac{r_a}{2}\right), \end{cases} \tag{9}$$

where J_0 is the Bessel function of order zero. Therefore, the case when the first surface is the first term of Eq. (9) is the plot (a) in Fig. 3, the case when the first surface is the second term of Eq. (9) is the plot (b) in Fig. 3 and so on.

The shapes presented in Fig. 3 are illustrative examples of the many examples computed in [13]. The general formula still gives a correct second surface in order to get a singlet lens free of spherical aberration. Please see Appendix A.

C. Performance of the Formula

The same surface is evaluated for different object distances, and the system shows the capacity to generate the solution such as the singlet is free of spherical aberration in the image point. In Fig. 4, we change t_b and keep fixed the sagitta $z_a = J_0(r_a)$. We find that the maximum diameter of the lens is proportional to t_b.

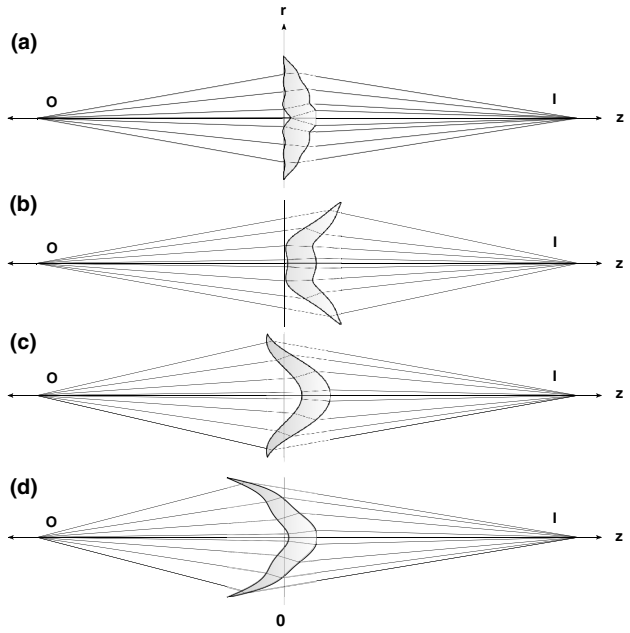

Fig. 3. Gallery of singlet lenses bi-aspherical free of spherical aberration. For all cases, the configuration is $t_a = -70$ mm, $t = 8$ mm, $t_b = 75$ mm, and $n = 1.5$.

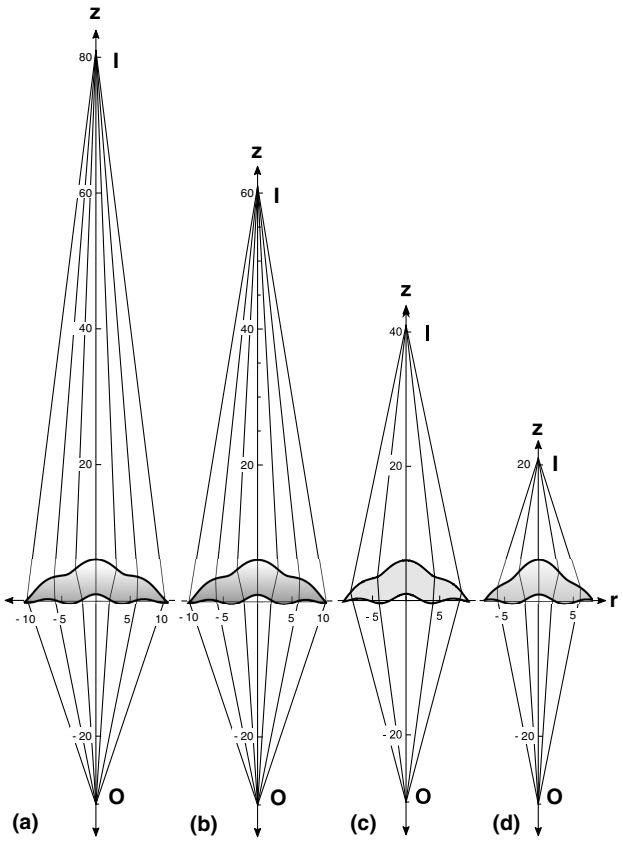

Fig. 4. (a) $t_b = 75$ mm, (b) $t_b = 55$ mm, (c) $t_b = 35$ mm, (d) $t_b = 15$ mm. The constant configuration of cases (a)–(d) is $t_a - 30$ mm, $t = 5$ mm, $n = 1.5$.

D. Example for Negative Refraction Index

In Fig. 5, the ray tracing can be seen for a lens with negative refraction index $n = -1.5$, for $z_a = J_0(r_a/2)$; therefore, we take the sign as $s_1 = -1$. It can be seen that for a negative refraction index, both sets Ω_a, Ω_b do not cross each other, $\Omega_a \cap \Omega_b = \varnothing$; therefore maximum radius tends to infinity.

E. Example When the Object Is at Minus Infinity

Now, when the object is far away, $t_a \to -\infty$, we need to compute the limit when $t_a \to -\infty$ for f_i, r_i, z_i, which can be written as

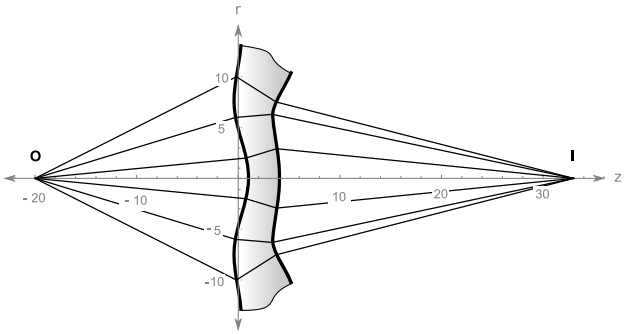

Fig. 5. Configuration of the singlet lens with negative refraction index: $t_a = -20$ mm, $t = 3$ mm, $t_b = 30$ mm, $n = -1.5$.

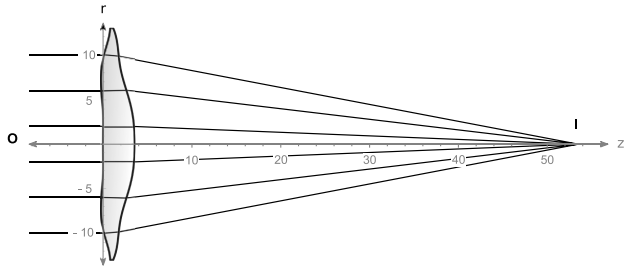

Fig. 6. Configuration of the singlet lens with object at infinity: $t = 3.5$ mm, $t_b = 50$ mm, $n = 1.5$.

$$\begin{cases} \lim\limits_{t_a \to -\infty} f_i = z_a - t_b, \\ \lim\limits_{t_a \to -\infty} z_i = \dfrac{\sqrt{\frac{(n^2-1)z_a'^2+n^2}{n^2(z_a'^2+1)}}}{\sqrt{z_a'^2+1}} + \dfrac{z_a'^2}{nz_a'^2+n}, \\ \lim\limits_{t_a \to -\infty} r_i = -\dfrac{z_a'\left(n\sqrt{z_a'^2+1}\sqrt{\frac{(n^2-1)z_a'^2+n^2}{n^2(z_a'^2+1)}}-1\right)}{n(z_a'^2+1)} \end{cases}. \tag{10}$$

Then, we can use Eq. (5) with the parameters of Eq. (10) and test it. For illustration proposes, we choose $z_a = \cos(r_a/2)r^2/200$ and plot the ray tracing in Fig. 6. From the figure, it is clear that the output rays converge to the image point despite $t_a \to \infty$.

F. Efficiency

To validate the efficiency of Eq. (5) we compare two vectors, $\boldsymbol{v}_3$ and $\boldsymbol{v}_3^\dagger$; $-\boldsymbol{v}_3$ comes from the image to the second surface, and $\boldsymbol{v}_3^\dagger$ is computed using Snell' law with the normal vector of the second surface, $\boldsymbol{n}_b$, and the unitary vector, $\boldsymbol{v}_2$ (Fig. 2); therefore, $\boldsymbol{n}_b$, $\boldsymbol{v}_3$, $\boldsymbol{v}_3^\dagger$ are written as

$$\begin{cases} \boldsymbol{n}_b = \dfrac{[z_b', -r_b', 0]}{\sqrt{z_b'^2+r_b'^2}}, \\ \boldsymbol{v}_3 = \dfrac{[r_b, z_b - t - t_b, 0]}{\sqrt{r_b^2+(z_b-t-t_b)^2}}, \\ \boldsymbol{v}_3^\dagger = n[\boldsymbol{n}_b \times (-\boldsymbol{n}_b \times \boldsymbol{v}_2)] - \boldsymbol{n}_b\sqrt{1 - n^2(\boldsymbol{n}_b \times \boldsymbol{v}_2)\cdot(\boldsymbol{n}_b \times \boldsymbol{v}_2)} \end{cases}. \tag{11}$$

The percentage efficiency of ray is measured how close ends in the image position, thus percentage efficiency is given by

$$E = 100\% - \left|\frac{\boldsymbol{v}_3^\dagger - \boldsymbol{v}_3}{\boldsymbol{v}_3}\right| \times 100\%. \tag{12}$$

We compute the efficiency for 550 rays for all the examples presented in the paper, and the average of all the examples is $99.99999999999986'\% \approx 100\%$. We believe that the error is not zero because the equations are very large, and when evaluated, we get computational errors such as truncation.

Please notice that for all examples, the singlets are free of spherical aberration even when the incident angles are very large; this happens because we do not use any paraxial approximation.

4. CONCLUSION

In this paper, we generalized the second surface in a lens in order to get an image free of spherical aberration for a given arbitrary first surface. When the first surface is such as the rays

inside the lens do not cross each other. We exhaustively test the formula by ray tracing, and we find that the solution presented works for positive and negative refractive indices. For a negative refraction index, we take $s_1 = -1$.

This general formula expands the variety of lenses free of spherical aberration. The efficiency of the method allows to design robust optical systems whose first surfaces are not restricted to the conical family functions.

APPENDIX A

We share the program code in Mathematica language to graph surfaces free of spherical aberration. The program is composed of three sections: the first one declares Eq. (5); in the second section, constants of the optical system are defined; finally, the graphing process is performed for the functions of the first surface and the second surface simultaneously.

Singlet free of spherical aberration.

```
(* Clean register. *)
Clear["Global'*"]

(* Define first surface function *)
za[ra_] := Module[{h}, h = Cos[ra 0.5]];

(* Define variables of Eq. (5) *)
Phi[ra_] := Module[{h},
      h = Sqrt[1 - (ra + (-ta + za[ra]) Derivative[1][za][ra])^2/
      (n^2 (ra^2 + (ta - za[ra])^2) (1 + (Derivative[1][za][ra])^2))]/
   Sqrt[1 + (Derivative[1][za][ra])^2]]

ri[ra_] := Module[{h},
   h = (ra + (-ta + za[ra]) Derivative[1][za][ra])/(
      n Sqrt[ra^2 + (ta - za[ra])^2] (1 + (Derivative[1][za][ra])^2)) -
      Derivative[1][za][ra] Phi[ra]]

zi[ra_] := Module[{h},
   h = (Derivative[1][za][
         ra] (ra + (-ta + za[ra]) Derivative[1][za][ra]))/(
      n Sqrt[ra^2 + (ta -
         za[ra])^2] (1 + (Derivative[1][za][ra])^2)) +Phi[
      ra]];

fi[ra_] := Module[{h}, h = ta - tb - Sign[ta] Sqrt[ra^2 + (ta - za
[ra])^2]];

h0[ra_] := Module[{h},
   h = ri[ra]^2 za[ra] + fi[ra] n zi[ra] -
      ra ri[ra] zi[ra] + (t + tb) zi[ra]^2 - n^2 (za[ra] + t zi[ra])];

h1[ra_] := Module[{h},
   h = ra^2 + 2 ra ri[ra] t + (tb - za[ra])^2 +
      t^2 (ri[ra]^2 + (-1 + zi[ra])^2) -
      2 t (tb - za[ra]) (-1 + zi[ra])];

zb[ra_] := Module[{h},
   h = (h0[ra] +
      s1 Sqrt[zi[ra]^2 (fi[ra]^2 -
         2 fi[ra] n (ra ri[ra] + ri[ra]^2 t +
            zi[ra] (t (zi[ra] - 1) - tb + za[ra])) +
         h1[ra] n^2 - (ra zi[ra] +
            ri[ra] (t + tb - za[ra]))^2)])/(-n^2 + 1)];

rb[ra_] := Module[{h}, h = ra + (ri[ra] (-za[ra] + zb[ra]))/zi[ra]];

(* Define system configuration's *)
s1 = 1;
n = 1.5;
t = 8;
ta = -60;
tb = 70;
basez = ta;
topez = tb + t;
rmax = 16.8; (* Iterative value *)

(* System plot *)
g1 = Plot[{za[ra], topez, basez}, {ra, -rmax, rmax},
   PlotStyle -> {Black, Transparent, Transparent},
   AspectRatio -> Automatic, AxesLabel -> {r, z}];
g2 = ParametricPlot[{rb[ra], zb[ra]}, {ra, -rmax, rmax},
   AspectRatio -> 1/1, AxesOrigin -> {0, 0}, PlotStyle ->
   {Black},
   Mesh -> None];
Show[g1, g2]
```

Please take care of the copy-paste process to avoid character coding errors between the pdf reader format and the mathematica work environment. We show the Code 1, Ref. [13].

Funding. Consejo Nacional de Ciencia y Tecnología (Conacyt) (593740).

REFERENCES

1. D. Malacara-Hernández and Z. Malacara-Hernández, *Handbook of Optical Design* (CRC Press, 2016).
2. R. K. Luneburg and M. Herzberger, *Mathematical Theory of Optics* (University of California, 1964).
3. D. Malacara, "Two lenses to collimate red laser light," Appl. Opt. **4**, 1652–1654 (1965).
4. E. M. Vaskas, "Note on the Wasserman–Wolf method for designing aspheric surfaces," J. Opt. Soc. Am. **47**, 669–670 (1957).
5. G. Wassermann and E. Wolf, "On the theory of aplanatic aspheric systems," Proc. Phys. Soc. London Sect. B **62**, 2–8 (1949).
6. P. D. Lin and C.-Y. Tsai, "Determination of unit normal vectors of aspherical surfaces given unit directional vectors of incoming and outgoing rays: reply," J. Opt. Soc. Am. A **29**, 1358 (2012).
7. J. C. Valencia-Estrada, R. B. Flores-Hernández, and D. Malacara-Hernández, "Singlet lenses free of all orders of spherical aberration," Proc. R. Soc. A **471**, 20140608 (2015).
8. J. C. Valencia-Estrada, M. V. Pereira-Ghirghi, Z. Malacara-Hernández, and H. A. Chaparro-Romo, "Aspheric coefficients of deformation for a Cartesian oval surface," J. Opt. **46**, 100–107 (2017).
9. M. Avendaño-Alejo, E. Román-Hernández, L. Castañeda, and V. I. Moreno-Oliva, "Analytic conic constants to reduce the spherical aberration of a single lens used in collimated light," Appl. Opt. **56**, 6244–6254 (2017).
10. G. Castillo-Santiago, M. Avendaño-Alejo, R. Daz-Uribe, and L. Castañeda, "Analytic aspheric coefficients to reduce the spherical aberration of lens elements used in collimated light," Appl. Opt. **53**, 4939–4946 (2014).
11. N. D. C. Lozano-Rincón and J. C. Valencia-Estrada, "Paraboloid-aspheric lenses free of spherical aberration," J. Modern Opt. **64**, 1146–1157 (2017).
12. J. C. Valencia-Estrada, J. Garca-Marquez, L. Chassagne, and S. Topsu, "Catadioptric interfaces for designing VLC antennae," Appl. Opt. **56**, 7559–7566 (2017).
13. R. G. González-Acuña and H. A. Chaparro-Romo, "Singlet free of spherical aberration," 2018, https://doi.org/10.6084/m9.figshare.7163357.